
Efficient Sparse Selective-Update RNNs for Long-Range Sequence Modeling

Bojian Yin¹ Shurong Wang^{1,2} Haoyu Tan³ Sander Bohte⁴ Federico Corradi³ Guoqi Li¹

Abstract

Real-world sequential signals, such as audio or video, contain critical information that is often embedded within long periods of silence or noise. While recurrent neural networks (RNNs) are designed to process such data efficiently, they often suffer from “memory decay” due to a rigid update schedule: they typically update their internal state at every time step, even when the input is static. This constant activity forces the model to overwrite its own memory and makes it hard for the learning signal to reach back to distant past events. Here we show that we can overcome this limitation using Selective-Update RNNs (suRNNs), a non-linear architecture that learns to preserve its memory when the input is redundant. By using a neuron-level binary switch that only opens for informative events, suRNNs decouple the recurrent updates from the raw sequence length. This mechanism allows the model to maintain an exact, unchanged memory of the past during low-information intervals, creating a direct path for gradients to flow across time. Our experiments on the Long Range Arena, WikiText, and other synthetic benchmarks show that suRNNs match or exceed the accuracy of much more complex models such as Transformers, while remaining significantly more efficient for long-term storage. By allowing each neuron to learn its own update timescale, our approach resolves the mismatch between how long a sequence is and how much information it actually contains. By providing a principled approach to managing temporal information density, this work establishes a new direction for achieving Transformer-level performance within the highly efficient framework of recurrent modeling.

1. Introduction

Recurrent Neural Networks (RNNs) are a classical and foundational framework for sequential modeling (Elman, 1990; Hopfield, 1982; McCulloch & Pitts, 1943). Theoretically, RNNs are capable of representing arbitrary state-dependent computations through Turing-complete recurrence (Kilian & Siegelmann, 1996; Keiblinger, 2025). Practically, RNNs are attractive for $\mathcal{O}(1)$ memory complexity during autoregressive inference and low-latency decoding, making them natural candidates for streaming, on-device, and ultra-long sequence deployment (Graves, 2012; Liu et al., 2019). Despite this elegant formulation and favorable inference efficiency, RNNs have been largely surpassed by Transformers (Vaswani et al., 2017b) and modern State Space Models (SSMs) (Gu et al., 2021a; Tay et al., 2022), particularly in tasks where capturing long-range dependencies is essential. Real-world sequential data (e.g., text, audio, or video) exhibit highly non-uniform information density: significant events are typically sparse and separated by long intervals of redundancy or noise. Ideally, a sequence model should allocate computation effort in proportion to information density rather than raw sequence length. However, many widely used models remain *information-agnostic* in this regard. For instance, Transformers compute pairwise interactions across time steps via $\mathcal{O}(L^2)$ attention map, while SSMs integrate history through long-range convolutions. Yet, these models have access to distant context but they process each time step uniformly, expending equal effort on informative and redundant content. RNNs face an even worse situation where they apply a dense, uniform, and *time-agnostic* transformation at every time step, forcing the valuable historical information to be constantly overwritten and re-encoded. This synchronization of computation with sequence length prevents the model from distinguishing meaningful transitions from non-informative ones, resulting in unnecessary state updates that are wasteful and can actively degrade long-term retention.

To bridge this mismatch, we propose **Selective-Update RNNs (suRNNs)** (Fig. 1a), an architecture designed to alleviate the long-term dependency problem through temporal sparsity at the neuron level. Our core insight is that stable long-sequence retention requires two properties: (i) an identity map to preserve states during non-informative intervals, and (ii) a mechanism to perform informative updates selectively. suRNNs instantiate these by replacing conven-

¹Institute of Automation, Chinese Academy of Sciences

²Zhejiang University ³Eindhoven University of Technology

⁴Machine Learning Group, Centrum Wiskunde & Informatica (CWI). Correspondence to: Bojian Yin <bojian.yin@ia.ac.cn>, Guoqi Li <guoqi.li@ia.ac.cn>.

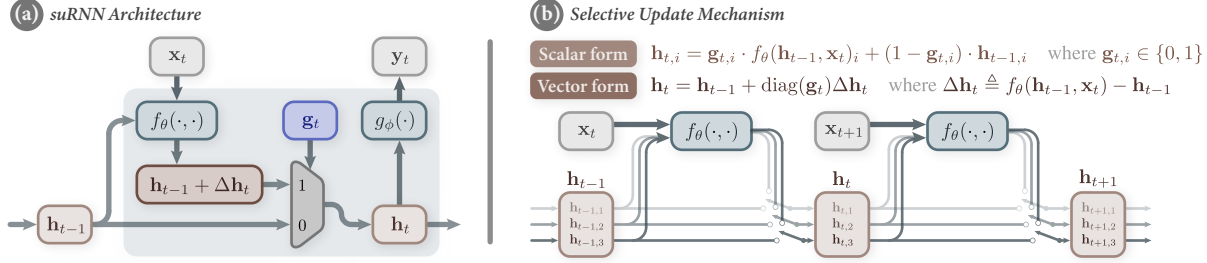


Figure 1. **suRNN architecture and the selective update mechanism:** (a) Transition of suRNN from time step $t - 1$ to t : unlike conventional RNNs that apply a uniform, time-agnostic transition, suRNN adopts a per-neuron, time-dependent binary gate $\mathbf{g}_t \in \{0, 1\}^H$. This allows each neuron to dynamically choose whether to preserve or update its state at each step. (b) Selective-update mechanism for $H = 3$ neurons: the per-neuron gating logic functions as an RC circuit with a switch. When the switch is off ($\mathbf{g}_{t,i} = 0$, bottom path), neuron $\mathbf{h}_{t,i}$ bypasses the update and remains unchanged; when the switch is on ($\mathbf{g}_{t,i} = 1$, top path), neuron $\mathbf{h}_{t,i}$ undergoes a standard non-linear update.

tional continuous gating with a time-dependent, neuron-wise binary gate $\mathbf{g}_{t,i} \in \{0, 1\}$, thereby decoupling effective recurrent updates from raw sequence. This modification directly overcomes the time-agnostic update schedule of conventional RNNs, and injects the temporal awareness to the model through diverse gating schedules. To handle the non-differentiability of the discrete gates, we adopt the Straight-Through Estimator (STE) (Bengio et al., 2013), drawing a direct parallel to surrogate gradient methods in Spiking Neural Networks (Neftci et al., 2019).

As depicted in Fig. 1b, selective update induces a dual-mode dynamics. When the gate is switched off ($\mathbf{g}_{t,i} = 0$), the i -th neuron acts as an ideal memory cell, preserving the exact same state from the previous time step; when the gate is switched on ($\mathbf{g}_{t,i} = 1$) for the i -th neuron, a standard nonlinear update is applied. Consequently, this mechanism induces a *sparse credit-assignment* effect, in which the number of non-identity transitions along a gradient path scales with the number of informative events (gate activations) rather than the raw sequence length.

Unlike prior adaptive computation approaches — such as the global halting logic of Adaptive Computation Time (Graves, 2016), the discrete step-skipping of Skip RNNs (Campos et al., 2018), or the rigid schedules of Clockwork RNNs (Koutník et al., 2014) — suRNNs implement sparsity at the finest possible resolution: the individual neuron. These earlier methods often struggle to scale to larger models and longer sequences, as they are hindered by the optimization instability of auxiliary ponder losses or the sequential bottlenecks of global control flow (Campos et al., 2018). By contrast, suRNNs integrate sparsity directly into the recurrent updates, enabling heterogeneous effective timescales to emerge naturally across the hidden state. This per-neuron selectivity avoids global contextual synchronization on all neurons, ensures stable training on large-scale datasets, and concentrates representational capacity exclusively on salient transitions. Our main contributions are as follows:

- **Selective Update Mechanism:** We introduce suRNN, an architecture that replaces continuous gating with binary selection to enable exact state preservation during intervals of informational stasis.
- **Sparse Credit Assignment:** We apply the STE to recurrent gating, inducing a functional gradient path that scales with the number of salient events rather than raw sequence length, effectively bypassing the vanishing/explosion gradient problem.
- **Strong Empirical Performance:** We show that suRNN outperforms existing RNNs in streaming tasks such as psMNIST, sCIFAR, and selective copy. Furthermore, suRNN matches or exceeds the accuracy of modern Transformers on the Long Range Arena (LRA) and WikiText benchmarks while maintaining $\mathcal{O}(1)$ inference efficiency.

2. Background

2.1. Recurrent Neural Network

Conceptually, recurrent neural networks (RNNs) map an input sequence $\{\mathbf{x}_t\}_{t=1}^T$ to hidden states $\{\mathbf{h}_t\}_{t=1}^T$, where $\mathbf{h}_t \in \mathbb{R}^H$ summarizes the history up to time t . A standard recurrent layer evolves according to:

$$\mathbf{h}_t = f_\theta(\mathbf{h}_{t-1}, \mathbf{x}_t), \quad \text{for } 1 \leq t \leq T, \quad (1)$$

where $f_\theta(\cdot, \cdot)$ is parameterized by θ and generates the next state \mathbf{h}_t from the previous state \mathbf{h}_{t-1} and input \mathbf{x}_t . At each time step t , a readout $\mathbf{y}_t = g_\phi(\mathbf{h}_t)$ is computed from the current hidden state \mathbf{h}_t , and a step-wise loss $\ell_t = \ell(\mathbf{y}_t, \mathbf{y}_t^*)$ measures the disagreement between \mathbf{y}_t and the ground truth \mathbf{y}_t^* . An overall loss $\mathcal{L}(\theta, \phi)$ can then be defined to measure the discrepancy between the model outputs $\{\mathbf{y}_t\}_{t=1}^T$ and the targets $\{\mathbf{y}_t^*\}_{t=1}^T$:

$$\mathcal{L}(\theta, \phi) = \sum_{t=1}^T \ell_t = \sum_{t=1}^T \ell(g_\phi(f_\theta(\mathbf{h}_{t-1}, \mathbf{x}_t)), \mathbf{y}_t^*) \quad (2)$$

Standard RNNs are time-agnostic in the sense that the same transition function f_θ is applied at every time step. Despite being parameter-efficient, this design can be restrictive under non-stationary or time-dependent dynamics, where the appropriate update rule should vary over time.

2.2. Backpropagation Through Time

Training RNNs requires minimizing the overall loss $\mathcal{L}(\theta, \phi)$. Since the loss \mathcal{L} involves the iterative states $\{\mathbf{h}_t\}_{t=1}^T$, it is typically optimized via BPTT, which unrolls hidden states backward in time:

$$\frac{\partial \mathcal{L}}{\partial \mathbf{h}_{t-1}} = \frac{\partial \mathcal{L}}{\partial \mathbf{h}_t} \frac{\partial \mathbf{h}_t}{\partial \mathbf{h}_{t-1}} + \frac{\partial \ell_t}{\partial \mathbf{h}_{t-1}} \quad (3)$$

Let $\mathbf{J}_t \triangleq \partial \mathbf{h}_t / \partial \mathbf{h}_{t-1} \in \mathbb{R}^{H \times H}$. Unrolling Eq. 3 shows that credit assignment across $t-s$ steps involves the product $\prod_{\tau=s+1}^t \mathbf{J}_\tau$. If $\|\mathbf{J}_\tau\| \leq \rho$ holds uniformly, then $\|\prod_{\tau=s+1}^t \mathbf{J}_\tau\| \leq \rho^{t-s}$, which implies that gradient vanishes when $\rho < 1$ and explodes when $\rho > 1$.

Therefore, the effective credit-assignment depth scales with sequence length, motivating architectures that reduce the multiplicative depth of backpropagation without changing the forward recurrence.

3. Methods

To address the above optimization issues, we propose Selective-Update RNNs (suRNNs), which replace continuous gating with a neuron-level binary mechanism. This shift enables exact identity mappings so that the hidden state can skip redundant updates and preserve information across long time spans.

3.1. Selective Update

Building on the standard recurrent update in Section 2.1, we introduce a per-neuron binary gate $\mathbf{g}_t \in \{0, 1\}^H$ with diagonal mask $\mathbf{D}_t = \text{diag}(\mathbf{g}_t)$ and reparameterize the state evolution of the recurrent network as:

$$\begin{aligned} \mathbf{h}_t &= \mathbf{h}_{t-1} + \mathbf{D}_t \Delta \mathbf{h}_t \\ &= \mathbf{h}_{t-1} + \mathbf{D}_t (f_\theta(\mathbf{h}_{t-1}, \mathbf{x}_t) - \mathbf{h}_{t-1}) \\ &= (\mathbf{I} - \mathbf{D}_t) \mathbf{h}_{t-1} + \mathbf{D}_t f_\theta(\mathbf{h}_{t-1}, \mathbf{x}_t). \end{aligned} \quad (4)$$

Here, $\Delta \mathbf{h}_t \in \mathbb{R}^H$ is the residual proposal, the deviation from identity produced by the original recurrent transformation, $\Delta \mathbf{h}_t \triangleq f_\theta(\mathbf{h}_{t-1}, \mathbf{x}_t) - \mathbf{h}_{t-1}$. When $\mathbf{g}_{t,i} = 0$, the i -th neuron (i.e., $\mathbf{h}_{t,i}$) is carried exactly, while the usual recurrent step is applied when $\mathbf{g}_{t,i} = 1$. This mechanism preserves the update rule f_θ and its parameters and controls only when f_θ is applied to each neuron. In a mask-aware implementation, neurons with $\mathbf{g}_{t,i} = 0$ need not contribute to $\Delta \mathbf{h}_t$, so the cost of the forward and backward passes

can scale with $\sum_{i=1}^H \mathbf{g}_{t,i} \leq H$ rather than H . In practice, selective update can accelerate inference when the learned gates are sufficiently sparse and the implementation exploits that sparsity.

Mathematically, linearizing the discrete map (4) around $(\mathbf{x}_t, \mathbf{h}_{t-1})$ gives the one-step Jacobian:

$$\mathbf{J}_t \triangleq \frac{\partial \mathbf{h}_t}{\partial \mathbf{h}_{t-1}} = \mathbf{I} + \mathbf{D}_t (\mathbf{J}_t^{(f)} - \mathbf{I}), \quad (5)$$

where $\mathbf{J}_t^{(f)} = \partial f_\theta / \partial \mathbf{h}_{t-1} |_{(\mathbf{h}_{t-1}, \mathbf{x}_t)}$ denotes the Jacobian of f_θ (Eq. 1). Eq. 5 mirrors the characteristic residual form $\mathbf{I} + \partial f / \partial \mathbf{x}$ as in ResNet (He et al., 2016), but now applied along the temporal axis. The identity term provides an exact carry route for gradients, and the diagonal mask \mathbf{D}_t projects the residual correction onto the active neurons only. In particular, if $\mathbf{g}_{t,i} = 0$, the i -th row of \mathbf{J}_t equals the corresponding row of \mathbf{I} , so no change or mixing occurs for the i -th neuron at time t . This row-wise identity property underpins the shorter gradient paths established in our analysis.

3.2. Gate Scheduling

We propose generating the gates \mathbf{g} with a *rhythmic* module:

$$a_{t,i} = b_i + \sum_{k=1}^K \alpha_{ik} \sin(\omega_k \cdot t + \phi_{i,k}), \quad \mathbf{g}_{t,i} = \mathbf{H}(a_{t,i}). \quad (6)$$

where $\mathbf{H}(\cdot)$ denotes the Heaviside step function. In this formulation, the K frequencies $\{\omega_k\}$ are shared across the layer, while the amplitudes α_{ik} , phases $\phi_{i,k}$, and biases b_i are learned per unit. By default, we set K equal to the hidden dimension H .

To facilitate end-to-end training through the non-differentiable Heaviside step function, we use a straight-through estimator (Bengio et al., 2013) or surrogate gradients (Nefci et al., 2019). During the forward pass, the model uses the discrete gate $\mathbf{g}_{t,i} = \mathbf{H}(a_{t,i}) = \mathbb{1}\{a_{t,i} > 0\}$, while the backward pass uses a surrogate gradient derived from a sigmoid function $\sigma(x)$.

For implementation efficiency, the frequencies ω_k are initialized on a logarithmic grid to span multiple orders of magnitude, and $\{\sin(\omega_k t)\}_{k=1}^K$ is precomputed, resulting in a marginal $\mathcal{O}(KH)$ computational overhead. Note that while this sinusoidal parameterization is effective for modeling structured intervals, the suRNN framework is agnostic to the gate generator; data-driven modules such as MLPs or SSMs can serve as drop-in alternatives without altering the underlying theoretical properties of the selective update.

Table 1. Most informative structural trade-offs of sequence layers. In this table, T is sequence length, d is hidden size, k is convolution kernel size, and $p \in [0, 1]$ is the update rate (Eq. 11). “Compute / layer” is worst-case training cost; “Sequential ops” counts inherently serial steps across time. “Effective non-identity depth” measures the typical number of non-identity transitions on a long-range route. “Streaming state” is memory required for strict online decoding, and “AR inference / token” is the per-token cost at context length n . The $\mathcal{O}(pn)$ and $\mathcal{O}(pd^2)$ entries assume a mask-aware implementation that skips inactive neurons; otherwise selective-update recurrence matches dense RNN worst-case cost.

Layer type	Compute / layer	Sequential ops	Effective depth	Streaming state	AR inference / token
Self Attention	$\mathcal{O}(T^2d)$	$\mathcal{O}(1)$	$\mathcal{O}(1)$	$\mathcal{O}(Td)$	$\mathcal{O}(Td)$
Conv $_k$	$\mathcal{O}(Tkd^2)$	$\mathcal{O}(1)$	$\mathcal{O}(\log_k T)$	$\mathcal{O}(kd)$	$\mathcal{O}(kd^2)$
RNN (dense)	$\mathcal{O}(Td^2)$	$\mathcal{O}(T)$	$\mathcal{O}(T)$	$\mathcal{O}(d)$	$\mathcal{O}(d^2)$
suRNN (ours)	$\mathcal{O}(Td^2)$	$\mathcal{O}(T)$	$\mathcal{O}(\bar{p}T)$	$\mathcal{O}(d)$	$\mathcal{O}(\bar{p}d^2)$

3.3. Selective update shortens effective gradient paths

Let $1 \leq s < t \leq T$. Following Eq. 5, the Jacobian of the unrolled computation map from \mathbf{h}_s to \mathbf{h}_t is

$$\frac{\partial \mathbf{h}_t}{\partial \mathbf{h}_s} = \prod_{\tau=s+1}^t \mathbf{J}_\tau = \prod_{\tau=s+1}^t (\mathbf{I} + \mathbf{D}_\tau(\mathbf{J}_\tau^{(f)} - \mathbf{I})), \quad (7)$$

which is exact for the forward trajectory $\{(\mathbf{h}_{\tau-1}, \mathbf{x}_\tau)\}_{\tau=s}^t$. For the i -th neuron, define the update set and count

$$\mathcal{U}(s, t) \triangleq \{\tau \in \mathbb{Z} \mid s < \tau \leq t\} \quad (8)$$

$$\mathcal{U}_i^{\text{on}}(s, t) \triangleq \{\tau \in \mathcal{U}(s, t) \mid \mathbf{g}_{\tau,i} = 1\} \quad (9)$$

When $\mathbf{g}_{\tau,i} = 0$, the i -th row of \mathbf{J}_τ equals the i -th row of \mathbf{I} and would not expand the multiplicative chain for the i -th neuron. Although BPTT still unrolls T times, identity carries make the non-identity factors in the gradient product scale with the number of informative updates $|\mathcal{U}_i^{\text{on}}(s, t)|$ rather than sequence length $|\mathcal{U}(s, t)|$.

Assumptions and norms Let $\|\cdot\|$ denote any submultiplicative matrix norm (e.g., the operator norm induced by ℓ_2 norm). Bounds below are stated for the *row-wise* sensitivity $\|\partial \mathbf{h}_{t,i} / \partial \mathbf{h}_s\|$, interpreted via the induced norm on the i -th row of the Jacobian.

Proposition 1 (effective path length) Assume $\|\mathbf{J}_\tau^{(f)}\| \leq \rho$ for all $\tau \in \mathcal{U}(s, t)$. For each neuron i there exists a constant C_i , independent of $t-s$, such that

$$\left\| \frac{\partial \mathbf{h}_{t,i}}{\partial \mathbf{h}_s} \right\| \leq C_i \rho^{|\mathcal{U}_i^{\text{on}}(s,t)|} < C_i \rho^{t-s}. \quad (10)$$

In a conventional RNN that every neuron updates every step, the analogous bound scales as ρ^{t-s} . Thus the exponent that governs vanishing or exploding depends on the *number of updates actually taken* by neuron i , not on elapsed steps. The constant C_i absorbs cross-neuron coupling at update times (off-diagonal contributions in the i -th row when $\mathbf{g}_{\tau,i} = 1$) and does not grow with the sequence length.

Effective depth scales with update rate Let \bar{p} be the *update rate*, which is the average number of times that the gate of each neuron is switched on for all time steps:

$$\bar{p} \triangleq \frac{1}{T} \sum_{i=1}^H |\mathcal{U}_i^{\text{on}}(0, T)| < 1 \quad (11)$$

Then, the expected number of informative updates performed on each neuron is $\bar{p}T < T$, so the effective depth scales with update rate \bar{p} rather than sequence length. Plugging this into Proposition 1 gives $\|\partial \mathbf{h}_T / \partial \mathbf{h}_0\| \lesssim C \rho^{\bar{p}T}$, which makes explicit that reducing the update rate slows both gradient vanishing and exploding.

Unlike the continuous gates in LSTMs (Hochreiter & Schmidhuber, 1997) and GRUs (Cho et al., 2014) that (1) subject the hidden state to persistent fractional updates and force the temporal correlations to be asymptotically overwritten by transitions and (2) merely scales the spectral radius ρ , the binary gates in suRNN fundamentally reduce the effective gradient depth to $1/\bar{p}$ times shorter than the raw sequence length. This discretization transforms the optimization landscape from one of persistent decay to one of selective preservation.

Backpropagation Combining Eq. 3 with the selective-update Jacobian in Eq. 5, the BPTT recursion becomes

$$\frac{\partial \mathcal{L}}{\partial \mathbf{h}_{t-1}} = \frac{\partial \mathcal{L}}{\partial \mathbf{h}_t} \left(\mathbf{I} + \mathbf{D}_t(\mathbf{J}_t^{(f)} - \mathbf{I}) \right) + \frac{\partial \ell_{t-1}}{\partial \mathbf{h}_{t-1}}. \quad (12)$$

non-update neurons propagate through an exact identity row: if $\mathbf{g}_{t,i} = 0$, the i -th row of $\mathbf{I} + \mathbf{D}_t(\mathbf{J}_t^{(f)} - \mathbf{I})$ equals the corresponding row of \mathbf{I} , so no change and no mixing occur for neuron i at time t . Consequently, parameter updates are sparse in time and in units:

$$\frac{\partial \mathcal{L}}{\partial \theta} = \sum_{t=1}^T \frac{\partial \mathcal{L}}{\partial \mathbf{h}_t} \mathbf{D}_t \frac{\partial f_\theta(\mathbf{x}_t, \mathbf{h}_{t-1})}{\partial \theta}, \quad (13)$$

so, only active units at update steps contribute to $\partial \mathcal{L} / \partial \theta$. Finally, when $\mathbf{g}_{t,i} = H(a_{t,i})$, the gradients reach the gate

generator via a straight-through surrogate for H, with local signal proportional to $(\frac{\partial \mathcal{L}}{\partial \mathbf{h}_{t,i}}) \Delta \mathbf{h}_{t,i}$.

For illustration, we revisit the classic Copying-Memory task (Le et al., 2015), where the model observes a short prefix, then T blanks and a delimiter, and must reproduce the prefix after the delimiter, stressing long-range dependency. For sequences with delay T , we track $\|\partial \ell / \partial \mathbf{h}_\tau\|$ as a function of temporal distance for both RNN and GRU, and their selective-update variants. With selective updates, in Fig. 2 a), gradient traces remain bounded and nearly parallel as T increases, consistent with the Jacobian structure $\mathbf{J}_t = \mathbf{I} + \mathbf{D}_t(\mathbf{J}_t^{(f)} - \mathbf{I})$ and Proposition 1, which predicts effective multiplicative depth governed by updates taken rather than input length. On task with $T = 5000$, the selective update gated models converge faster and reach a lower loss, and PCA trajectories (in Fig A3 in Appendix) show more structured state dynamics with clearer separation between delay and recall than a standard GRU.

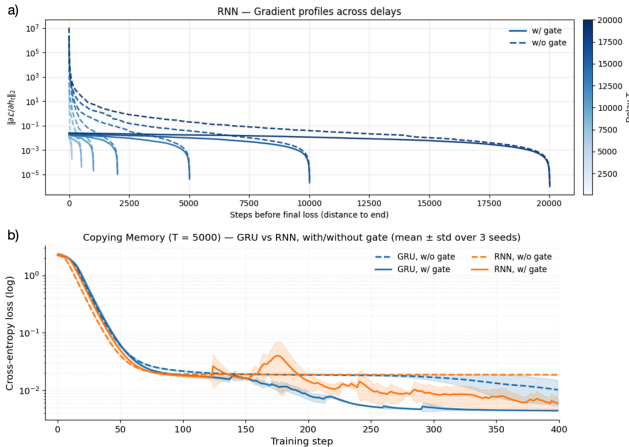


Figure 2. Selective update improves long-range credit assignment. (a) RNN gradient profiles across delays T (color bar; solid = with selective gate, dashed = without). Gating keeps gradients bounded (about $10^{-3} - 10^{-2}$, log scale) with near-parallel decay; increasing T mainly stretches the horizon, while ungated runs collapse to a tiny floor after early spikes. (b) Copying Memory at $T=5000$ (mean \pm std over 3 seeds): both GRU and RNN with the gate converge faster and to lower loss, whereas ungated baselines plateau. These trends indicate the gate acts as an identity/skip path with per-step gain near 1, preserving long-range gradients.

Selective update creates ensembles of sub-RNNs By expanding the product $\prod_{\tau=s+1}^t \mathbf{J}_\tau$ in Eq. 7:

$$\prod_{\tau=s+1}^t (\mathbf{I} + \mathbf{D}_\tau(\mathbf{J}_\tau^{(f)} - \mathbf{I})) = \sum_{S \subseteq \mathcal{U}(s,t)} \prod_{\tau_i \in S} \mathbf{D}_{\tau_i}(\mathbf{J}_{\tau_i}^{(f)} - \mathbf{I}), \quad (14)$$

corresponding to distinct computation paths that apply the non-identity transform only on the selected timesteps and otherwise follow identity carries. On the computational

graph, each particular gate realization therefore selects a sparse subgraph of the full unrolled RNN, yielding a sub-RNN that operates on a subsequence of updates; across inputs and layers, the model effectively integrates many such subgraphs (Graves, 2016). This many-path view clarifies why selective updates can preserve functional depth while providing abundant short, identity-rich routes for gradient flow, paralleling the ensemble interpretation of residual networks (Veit et al., 2016).

In essence, selective updates increase usable memory, not memory capacity, by changing how information is preserved and how credit is assigned over time. It is enlarging the state by decoupling retention and credit assignment from un-selected timesteps. Non-updating neurons are carried exactly, avoiding repeated mixing and drift, and gradients traverse identity routes during these intervals. Consequently, effective temporal depth is governed by the number of selected subsequence rather than the whole sequence, yielding longer-lived representations and better-conditioned BPTT.

3.4. Implementation

Selective updates are a lightweight reparameterization and can be applied to essentially any recurrent backbone by inserting an identity-through-time carry with a learned temporal mask, without changing the underlying recurrent transform (Fig A1 in Appendix). However, a direct stepwise realization still requires time consuming BPTT, which becomes a practical bottleneck as model size and context length grow. To enable scalable experiments, we introduce suGRU, a selective-update variant of the *CUDA-fused* GRU that preserves execution speed, without any custom kernels or single-step control flow with minimal overhead. Implementation details are provided in Appendix B.

Efficiency Beyond scalability, selective update improves both latency and memory traffic by skipping their recurrent computations and associated reads/writes under mask-aware execution. While this conditional execution is not supported by default in PyTorch kernels, we use a mask-aware C implementation of stepwise suGRU with block gating on sequential MNIST, we measure a $5.3\times$ latency reduction at 83% sparsity (466 ms \rightarrow 88 ms per step; details in the Appendix D.0.3). This event-triggered computation is naturally compatible with sparse-kernel, neuromorphic, and other event-driven hardware that supports conditional state updates.

4. Experiments

We evaluate the efficacy of Selective-Update RNNs on a comprehensive suite of long-range benchmarks, ranging from the Long Range Arena (LRA) and pixel-level classifi-

Table 2. **Long Range Arena (LRA) Results.** We compare suGRU against Transformer variants and State Space Models (S4). The **Streaming?** column indicates strictly uni-directional, streaming processing. Reported results are taken from (Gu et al., 2022)

MODEL	Streaming ?	LISTOPS	TEXT	RETRIEVAL	IMAGE	PATHFINDER	AVG
Transformer	No	36.37	64.27	57.46	42.44	71.40	53.66
Reformer	No	<u>37.27</u>	56.10	53.40	38.07	68.50	50.56
BigBird	No	36.05	64.02	59.29	40.83	74.87	54.17
Linear Trans.	No	16.13	<u>65.90</u>	53.09	42.34	75.30	50.46
Performer	No	18.01	65.40	53.82	42.77	77.05	51.18
FNet	No	35.33	65.11	59.61	38.67	77.80	54.42
Nyströmformer	No	37.15	65.52	79.56	41.58	70.94	57.46
Luna-256	No	37.25	64.57	79.29	<u>47.38</u>	77.72	59.37
S4	No	<u>59.60</u>	<u>86.82</u>	<u>90.90</u>	<u>88.65</u>	<u>94.20</u>	<u>86.09</u>
suGRU(binary new)	Yes	44.93	64.42	77.54	80.32	84.92	70.43
suGRU(sigmoid)	Yes	39.45	64.17	63.23	56.92	73.45	59.44

cation to synthetic memory tasks.

4.1. Long Range Arena

In the LRA benchmark suite (Tay et al., 2020), which comprises five tasks with sequence lengths ranging from 1K to 4K steps across multiple modalities and objectives (e.g., similarity matching, structural inference, and visuospatial reasoning), we compare suGRU against 8 Transformer variants and modern linear RNNs (e.g., S4,) as well as more recent methods reported in the literature. As summarized in Table 2, while models like S4 and LRU (Orvieto et al., 2023) achieve state-of-the-art accuracy on LRA (94% on Pathfinder), they often utilize bidirectional processing or global convolutions for these spatial classification tasks. In contrast, suGRU operates under a strict uni-directional (causal) constraint, processing the sequence strictly token-by-token without access to future context. Despite this handicap, suGRU achieves 84.92% on Pathfinder, significantly outperforming RWKV-v4 (58.42%) (Peng et al., 2023) and standard causal RNNs which typically fail this task. Ablation results confirm that binary gating decisively outperforms the continuous (sigmoid) alternative.

4.2. Selective copy

We evaluate suGRU on the Selective Copy task (Gu & Dao, 2024), a long range synthetic benchmark that requires reading a stream, selecting a small subset of marked symbols, and reproducing them after a long distractor interval ($T = 4096$), making the ideal computation pattern “sparse write, long carry”. While, selective updates implement this pattern directly: suGRU can *write* only at marked events and use an *exact carry* ($g_t = 0$) through distractors, reducing cumulative state drift and preserving gradient flow. As shown in Table 3, selective copy performance is strongly architecture-dependent: Hyena (Poli et al., 2023) variants

Table 3. **Selective Copy** accuracy across models and configurations. Here, L denotes the number of layers. Reported values are taken from (Feng et al., 2024)

Model	Layer	Accuracy
H3	Hyena	30.1
Mamba	Hyena	28.4
S4	S4	18.3
H3	S4	57.0
Mamba	S4	56.4
S4	S6	97.0
H3	S6	99.7
Mamba	S6	99.8
GRU	S4(2L)	16.3 ± .5
suGRU	S4(2L)	97.2 ± .3
suGRU	S4(3L)	99.5 ± .5

are near chance, S4 (Gu et al., 2022) improves but remains below this setting, while S6 (Gu & Dao, 2023) reaches near-perfect accuracy. suGRU is competitive with these strong baselines while remaining strictly streaming: with an S4-style backbone, two layers attain 97.2% accuracy, and three layers reach 99.5%. This supports our claim that selective updates substantially improve long-sequence credit assignment, and that modest recurrent depth closes the remaining gap.

4.3. WikiText-103

WikiText-103 (Merity et al., 2017) is an established benchmark for language modeling, an important task for large-scale sequence models where tokens are predicted sequentially based on past context. Although RNNs were the model of choice for many years, Transformers are now the dominant model in such applications that contain data that is inherently discrete. We show that sequential RNN models trained via BPTT can still be competitive to Transformers

Table 4. Language modeling performance on WikiText-103. Top rows report baseline results are from (Qin et al.); bottom rows show our suGRU implementation performance.

Model	val PPL (\downarrow)	test PPL (\downarrow)	Params (M)
Transformer	24.40	24.78	44.65
FLASH	25.92	26.70	42.17
Performer	62.50	63.16	44.65
gMLP	28.08	29.13	47.83
S4	38.34	39.66	45.69
RWKV-4	24.31	25.07	46.23
LRU	29.86	31.12	46.24
Mamba	22.58	23.19	44.39
HGRN2	23.10	23.73	44.66
Transformer	18.32	18.44	44.65
suGRU	19.28	19.20	44.86
suGRU(100M)	18.29	18.29	88.98
Hybrid-GRU	18.07	18.03	48.92

in these settings.

As a result, suGRU significantly narrows the performance gap between purely recurrent architectures and attention-based baselines. Under a parameter-matched setting (Table 4, bottom), suGRU achieves a test perplexity of 21.53, while scaling the model to 100M parameters further reduces perplexity to 18.29. To further enhance performance, we introduce a hybrid architecture that interleaves suGRU layers with classical self-attention. This **Hybrid-suGRU** variant reaches a perplexity of 18.03 with only a marginal increase in parameter count, demonstrating that selective-update recurrence remains highly competitive at the language-modeling scale. As illustrated in Figure 3, both suGRU and the hybrid variant exhibit optimization stability and convergence rates on par with the Transformer baseline.

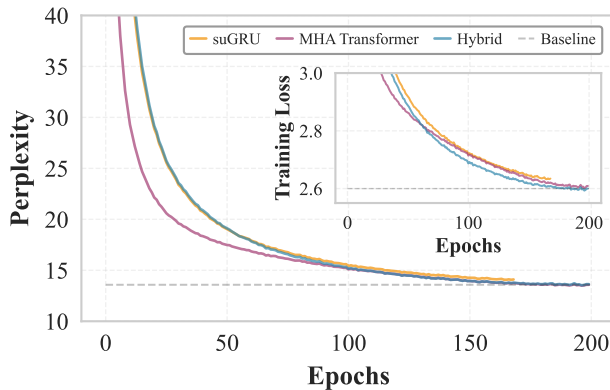


Figure 3. WikiText-103 language modeling learning curves showing training perplexity versus epochs for one-pass suGRU, a Hybrid variant, and a multi-head attention Transformer. The inset reports training loss over the same training run. The dashed horizontal line indicates the baseline transformer performance.

4.4. Pixel-level classification and analysis

We conducted more studies on pixel-level classification, from sequential MNIST and permuted variants to sequential CIFAR10.

Performance On these tasks, suGRU performs strongly under strict sequential training and decoding (Table 5). It matches the best reported accuracy on sMNIST and achieves competitive performance on psMNIST, comparable to Transformer results while retaining constant-memory recurrence. On the sCIFAR task, suGRU substantially outperforms the Transformer baseline and prior recurrent models. We prioritize comparison with LSSL (Gu et al., 2021b) as it represents a more direct, causal SSM baseline that shares our unidirectional, continuous-time modeling constraints. In addition, suGRU learns faster in these settings, converging in fewer epochs than standard GRU baselines, consistent with the shorter effective credit-assignment paths induced by selective updates. The learning curve and ablations over gate-scheduling variants are reported in the Appendix.

Other recurrent baselines. We evaluate selective updates across several recurrent backbones on psMNIST, including vanilla RNNs, GRU, LSTM, and representative spiking models. Table A1 in Appendix shows consistent improvements over the corresponding non-selective architectures: su-RNN, su-GRU, and su-LSTM substantially outperform their standard counterparts and exceed a range of strong recurrent baselines. Our results show that su-GRU achieves the highest test accuracy among all reported streaming recurrent models. With Selecting Updating applied to SNNs as su-SNN, we establish a new state with 97.33% accuracy on testset (see Appendix Table A1), surpassing specialized spiking baselines such as Rhythm-SNNs (Yan et al., 2025) and Balanced Resonate-and-Fire Neurons (Higuchi et al., 2024).

Feature Visualization Figure 4 contrasts update timing (gates) with update magnitude (state increments) along the input stream. Gates form a stable, layer-dependent schedule with a moderate opening rate, largely consistent across digits. Increments Δh_t are concentrated at edge transitions and high-contrast changes, while background regions produce near-carry behavior. The second layer exhibits more distributed updates than the first, consistent with deeper recurrence integrating local evidence into higher-level state changes.

5. Related work

Residual connections address the optimization difficulties of very deep networks by making identity propagation the default and learning only deviations, which creates short gradient routes through depth and mitigates degradation as layers increase (He et al., 2016; Veit et al., 2016). At-

Table 5. Pixel-level 1-D image classification. Comparison against reported test accuracies from prior works (Gu et al., 2022).

	sMNIST	psMNIST	sCIFAR
Transformer	98.9	97.9	62.2
LSTM	98.9	95.11	63.01
r-LSTM	98.4	95.2	72.2
UR-LSTM	99.28	96.96	71.00
UR-GRU	99.27	96.51	74.4
HiPPO-RNN	98.9	98.3	61.1
LMU-FFT	–	98.49	–
LipschitzRNN	99.4	96.3	64.2
TCN	99.0	97.2	–
TrellisNet	99.20	98.13	73.42
CKConv	99.32	98.54	63.74
LSSL	99.53	98.76	84.65
suGRU	99.53	98.46	87.26

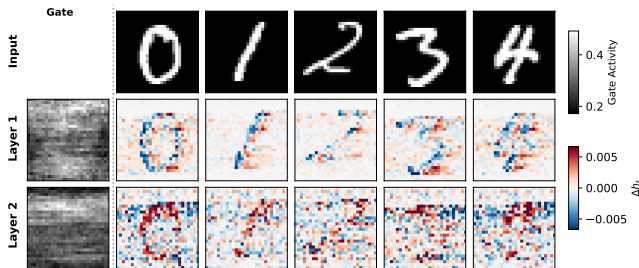


Figure 4. Spatio-temporal dynamics of a two-layer suGRU on sMNIST. Averaged gating activity (left) and hidden state changes $\Delta \mathbf{h}_t = \mathbf{h}_t - \mathbf{h}_{t-1}$ (right) are reshaped to 28×28 for spatial analysis. The signed increment maps demonstrate that the model performs sparse, event-triggered updates targeted at salient features in both layers, successfully bypassing redundant pixels.

tion offers an analogous benefit in sequence models by shortening token-to-token credit assignment with direct interactions rather than long temporal chains (Vaswani et al., 2017a). Our work follows the same principle along the temporal axis of recurrence, aiming to reduce the number of nontrivial transformations that gradients must traverse while preserving a strictly streaming recurrent computation.

Several recurrent research lines incorporate temporal residual structure, but they differ in how identity is introduced and in what is being optimized. Traditional additive temporal residual and highway-style RNNs (Srivastava et al., 2015) increase trainability by introducing skip pathways across depth or time while still applying a recurrent transform at every step, and stochastic carry regularizers such as Zoneout (Krueger et al., 2017) encourage partial identity behavior but do not explicitly control when computation is executed. As noted earlier, the second line explicitly learns to skip updates, including Adaptive Computation Time (Graves, 2016) and Skip RNN (Campos et al., 2018), as well as multi-rate schedules such as Clockwork RNN

(Koutník et al., 2014), Phased LSTM (Neil et al., 2016), and hierarchical multiscale RNNs (Chung et al., 2017). These methods typically gate whole-state updates or introduce halting and regularization objectives to balance accuracy and compute, and they often rely on sensitive training heuristics or fixed scheduling assumptions. In contrast, our selective updates introduce per-unit identity-through-time carries, preserve the base recurrent transform, and admit a direct path-length analysis in terms of updates.

6. Discussion and Conclusion

We introduced Selective-Update RNNs (suRNNs) to mitigate memory decay by decoupling update frequency from sequence length via binary gating. This mechanism is inspired by biological models of working memory, where frontostriatal circuits explicitly learn when to update internal representations versus maintain them (Frank et al., 2001; Chatham et al., 2014; Bhandari et al., 2018).

A key contribution of this work is demonstrating strong performance under strict *uni-directional* (causal) constraints. While non-causal State Space Models (e.g., S4, Mamba) excel on the Long Range Arena by leveraging non-causal convolutions or bi-directional views, suGRU operates as a strictly uni-directional streaming model. Our 84.92% accuracy on PATHFINDER shows that strictly causal RNNs can capture complex long-range spatial dependencies if the vanishing gradient problem is structurally mitigated. By implementing this theoretical improvement via a cuDNN fusion, we demonstrated that biologically plausible sparsity can be implemented without sacrificing hardware efficiency.

Our results suggest three directions for future research. First, we relied on standard GRU backbones to isolate the gating effect; more expressive recurrent parameterizations or context-aware gate generators could further raise the performance ceiling. Second, training still relies on BPTT, which remains a bottleneck for extreme lengths; future work should explore event-driven backpropagation or sparse checkpointing to better exploit temporal sparsity during optimization. Third, extending selective updates to bi-directional architectures could enhance performance for non-causal tasks with global context. Finally, the induced subnetwork structure suggests a natural connection to continual learning (Kang et al., 2022), where separating updates across contexts could reduce interference between tasks. Ultimately, taking inspiration from the biological principle of selective maintenance with the hardware efficiency of one-pass recurrence, suRNNs re-establish the viability of strict streaming architectures for long-context learning.

References

- Bengio, Y., Léonard, N., and Courville, A. Estimating or propagating gradients through stochastic neurons for conditional computation, 2013.
- Bhandari, A. et al. Learning and transfer of working memory gating policies. *Cognition*, 172:89–100, 2018. doi: 10.1016/j.cognition.2017.12.001.
- Campos, V., Jou, B., Giró-i Nieto, X., Torres, J., and Chang, S.-F. Skip rnn: Learning to skip state updates in recurrent neural networks. In *International Conference on Learning Representations*, 2018.
- Chatham, C. H., Frank, M. J., and Badre, D. Corticostriatal output gating during selection from working memory. *Neuron*, 81(4):930–942, 2014. doi: 10.1016/j.neuron.2014.01.002.
- Cho, K., van Merriënboer, B., Gulcehre, Ç., Bahdanau, D., Bougares, F., Schwenk, H., and Bengio, Y. Learning phrase representations using rnn encoder–decoder for statistical machine translation. In *Proceedings of EMNLP*, pp. 1724–1734, 2014. URL <https://aclanthology.org/D14-1179/>.
- Chung, J., Ahn, S., and Bengio, Y. Hierarchical multiscale recurrent neural networks. In *International Conference on Learning Representations (ICLR)*, 2017.
- Elman, J. L. Finding structure in time. *Cognitive science*, 14(2):179–211, 1990.
- Feng, L., Tung, F., Ahmed, M. O., Bengio, Y., and Hajimirsadeghi, H. Were rnns all we needed? *arXiv preprint arXiv:2410.01201*, 2024.
- Frank, M. J., Loughry, B., and O’Reilly, R. C. Interactions between frontal cortex and basal ganglia in working memory: a computational model. *Cognitive, Affective, and Behavioral Neuroscience*, 1(2):137–160, 2001. doi: 10.3758/cabn.1.2.137.
- Graves, A. Sequence transduction with recurrent neural networks. *arXiv preprint arXiv:1211.3711*, 2012.
- Graves, A. Adaptive computation time for recurrent neural networks. *arXiv preprint arXiv:1603.08983*, 2016.
- Gu, A. and Dao, T. Mamba: Linear-time sequence modeling with selective state spaces. *arXiv:2312.00752*, 2023. URL <https://arxiv.org/abs/2312.00752>.
- Gu, A. and Dao, T. Mamba: Linear-time sequence modeling with selective state spaces. In *International Conference on Learning Representations (ICLR)*, 2024. URL <https://openreview.net/forum?id=AL1fq05o7H>.
- Gu, A., Goel, K., and Ré, C. Efficiently modeling long sequences with structured state spaces. *arXiv:2111.00396*, 2021a. URL <https://arxiv.org/abs/2111.00396>.
- Gu, A., Johnson, I., Goel, K., Saab, K., Dao, T., Rudra, A., and Ré, C. Combining recurrent, convolutional, and continuous-time models with linear state space layers. *Advances in neural information processing systems*, 34: 572–585, 2021b.
- Gu, A., Goel, K., and Ré, C. Efficiently modeling long sequences with structured state spaces. In *International Conference on Learning Representations (ICLR)*, 2022. URL <https://openreview.net/forum?id=uYLFoz1vlAC>.
- He, K., Zhang, X., Ren, S., and Sun, J. Deep residual learning for image recognition. In *Proceedings of CVPR*, pp. 770–778, 2016. URL https://www.cv-foundation.org/openaccess/content_cvpr_2016/papers/He_Deep_Residual_Learning_CVPR_2016_paper.pdf.
- Higuchi, S., Kairat, S., Bohte, S., and Otte, S. Balanced resonate-and-fire neurons. In *International Conference on Machine Learning*, pp. 18305–18323. PMLR, 2024.
- Hochreiter, S. and Schmidhuber, J. Long short-term memory. *Neural Computation*, 9(8):1735–1780, 1997. doi: 10.1162/neco.1997.9.8.1735. URL <https://direct.mit.edu/neco/article/9/8/1735/6109/Long-Short-Term-Memory>.
- Hopfield, J. J. Neural networks and physical systems with emergent collective computational abilities. *Proceedings of the national academy of sciences*, 79(8):2554–2558, 1982.
- Kang, H., Mina, R. J. L., Madjid, S. R. H., Yoon, J., Hasegawa-Johnson, M., Hwang, S. J., and Yoo, C. D. Forget-free continual learning with winning subnetworks. In *International conference on machine learning*, pp. 10734–10750. PMLR, 2022.
- Keiblinger, M. Recurrence-complete frame-based action models. *arXiv preprint arXiv:2510.06828*, 2025.
- Kilian, J. and Siegelmann, H. T. The dynamic universality of sigmoidal neural networks. *Information and computation*, 128(1):48–56, 1996.
- Koutník, J., Greff, K., Gomez, F., and Schmidhuber, J. A clockwork RNN. In *Proceedings of the 31st International Conference on Machine Learning (ICML)*, volume 32 of *Proceedings of Machine Learning Research*, pp. 1863–1871, 2014.

- Krueger, D., Maharaj, T., Kramár, J., Pezeshki, M., Ballas, N., Ke, N. R., Goyal, A., Bengio, Y., and Courville, A. Zoneout: Regularizing RNNs by randomly preserving hidden activations. In *International Conference on Learning Representations (ICLR)*, 2017.
- Le, Q. V., Jaitly, N., and Hinton, G. E. A simple way to initialize recurrent networks of rectified linear units. *arXiv preprint arXiv:1504.00941*, 2015.
- Liu, L., Wang, H., Lin, J., Socher, R., and Xiong, C. Mkd: a multi-task knowledge distillation approach for pretrained language models. *arXiv preprint arXiv:1911.03588*, 2019.
- McCulloch, W. S. and Pitts, W. A logical calculus of the ideas immanent in nervous activity. *The bulletin of mathematical biophysics*, 5(4):115–133, 1943.
- Merity, S., Xiong, C., Bradbury, J., and Socher, R. Pointer sentinel mixture models. In *International Conference on Learning Representations (ICLR)*, 2017.
- Neftci, E. O., Mostafa, H., and Zenke, F. Surrogate gradient learning in spiking neural networks. *arXiv preprint arXiv:1901.09948*, 2019.
- Neil, D., Pfeiffer, M., and Liu, S.-C. Phased LSTM: Accelerating recurrent network training for long or event-based sequences. In *Advances in Neural Information Processing Systems*, volume 29, 2016.
- Orvieto, A., Smith, S. L., Gu, A., Fernando, A., Gulcehre, C., Pascanu, R., and De, S. Resurrecting recurrent neural networks for long sequences. In *International Conference on Machine Learning*, pp. 26670–26698. PMLR, 2023.
- Peng, B., Alcaide, E., Anthony, Q., Albalak, A., Arcadinho, S., Biderman, S., Cao, H., Cheng, X., Chung, M., Grella, M., et al. Rwkv: Reinventing rnnns for the transformer era. In *Findings of the Association for Computational Linguistics: EMNLP 2023*, pp. 14048–14077, 2023.
- Poli, M., Massaroli, S., Nguyen, E., Fu, D. Y., Dao, T., Baccus, S., Bengio, Y., Ermon, S., and Ré, C. Hyena hierarchy: Towards larger convolutional language models. In *International Conference on Machine Learning*, pp. 28043–28078. PMLR, 2023.
- Qin, Z., Yang, S., Sun, W., Shen, X., Li, D., Sun, W., and Zhong, Y. Hgrn2: Gated linear rnnns with state expansion. In *First Conference on Language Modeling*.
- Srivastava, R. K., Greff, K., and Schmidhuber, J. Highway networks, 2015.
- Tay, Y., Dehghani, M., Abnar, S., Shen, Y., Bahri, D., Pham, P., Rao, J., Yang, L., Ruder, S., and Metzler, D. Long range arena: A benchmark for efficient transformers. *arXiv preprint arXiv:2011.04006*, 2020.
- Tay, Y., Dehghani, M., Bahri, D., and Metzler, D. Efficient transformers: A survey. *ACM Computing Surveys*, 55(6):1–28, 2022. doi: 10.1145/3530811. URL <https://dl.acm.org/doi/10.1145/3530811>.
- Vaswani, A., Shazeer, N., Parmar, N., Uszkoreit, J., Jones, L., Gomez, A. N., Kaiser, Ł., and Polosukhin, I. Attention is all you need. In *Advances in Neural Information Processing Systems (NeurIPS)*, 2017a. URL <https://arxiv.org/abs/1706.03762>.
- Vaswani, A., Shazeer, N., Parmar, N., Uszkoreit, J., Jones, L., Gomez, A. N., Kaiser, Ł., and Polosukhin, I. Attention is all you need. *Advances in neural information processing systems*, 30, 2017b.
- Veit, A., Wilber, M., and Belongie, S. Residual networks behave like ensembles of relatively shallow networks. *arXiv:1605.06431*, 2016. URL <https://arxiv.org/abs/1605.06431>.
- Yan, Y., Yang, Q., Wu, Y., Liu, H., Zhang, M., Li, H., Tan, K. C., and Wu, J. Efficient and robust temporal processing with neural oscillations modulated spiking neural networks. *Nature communications*, 16(1):8651, 2025.

	RNN	GRU	SNN
Original Update	$\Delta h_t = \phi(W_{xh_t} x[t] + W_{hh_t} h[t-1] + b_{h_t}),$ $\bar{h}_t[t] = h_t[t-1] + \Delta h_t$ $\Rightarrow h_t[t] = \bar{h}_t[t]$	$z_t[t] = \sigma(W_{xz} x[t] + U_z h[t-1] + b_z),$ $r_t[t] = \sigma(W_{rx} x[t] + U_r h[t-1] + b_r),$ $\bar{h}_t[t] = \tanh(W_{\bar{h}} x[t] + U_{\bar{h}} (r_t[t] \odot h[t-1]) + b_{\bar{h}}),$ $\tilde{h}_t[t] = (1 - z_t[t]) h_t[t-1] + z_t[t] \odot \bar{h}_t[t]$ $\Rightarrow h_t[t] = \tilde{h}_t[t]$	$\Delta u_t = (W_{xh_t} x[t] + b_{h_t}),$ $\bar{u}_t[t] = \alpha u_t[t-1] + \Delta u_t - s_t[t-1] \theta$ $\Rightarrow u_t[t] = \bar{u}_t[t]$ $s_t[t] = \mathbf{H}(u_t[t] - \theta)$
Selective Update	$\Rightarrow h_t[t] = (1 - g_t[t]) h_t[t-1] + g_t[t] \bar{h}_t[t]$ $\Rightarrow h_t[t] = h_t[t-1] + g_t[t] \Delta h_t[t]$	$\Rightarrow h_t[t] = (1 - g_t[t]) h_t[t-1] + g_t[t] \tilde{h}_t[t]$ $\Rightarrow h_t[t] = (1 - g_t[t] z_t[t]) h_t[t-1] + g_t[t] z_t[t] \tilde{h}_t[t]$ $\Rightarrow h_t[t] = h_t[t-1] + g_t[t] z_t[t] (\tilde{h}_t[t] - h_t[t-1])$	$\Rightarrow u_t[t] = (1 - g_t[t]) u_t[t-1] + g_t[t] \bar{u}_t[t]$ $\Rightarrow u_t[t] = u_t[t-1] + g_t[t] (\bar{u}_t[t] - u_t[t-1])$

Figure A1. **Selective-update across recurrent families.** Top: the update equations for vanilla RNN, GRU, and a spiking neuron model (SNN). Bottom: the same modules rewritten in selective-update form by inserting a per-unit gate $g_i[t]$. In GRU, it composes with the native continuous gate $z_i[t]$, and in SNN it acts on membrane integration. This exposes a unified timing control across architectures while leaving the underlying transforms unchanged.

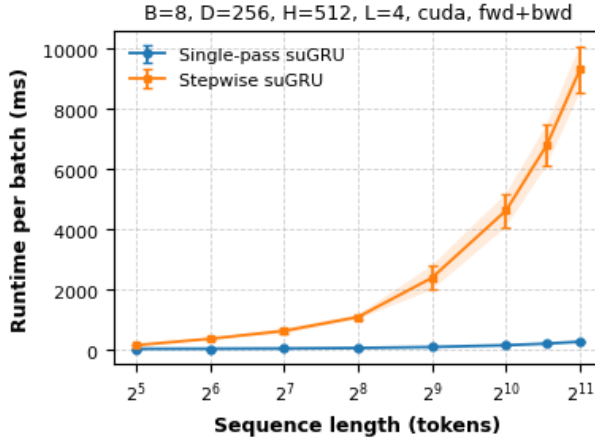


Figure A2. Runtime per batch (ms) versus sequence length for two suGRU implementations. **Single-pass suGRU** runs the entire sequence in one cuDNN GRU call using the skip-drive input, yielding near-flat scaling and substantially lower wall-clock time at long sequences. **Stepwise suGRU** applies per-step control flow and incurs rapidly growing cost. Error bars indicate run-to-run variation.

A. su-RNNs

Figure A1 demonstrates the universality of the selective-update mechanism across three distinct recurrent families: the vanilla RNN, the Gated Recurrent Unit (GRU), and the Spiking Neural Network (SNN). In each architecture, the binary gate $g_i[t]$ acts as a residual switch that arbitrates between the standard state evolution and an exact identity carry. For the RNN, it gates the non-linear residual Δh_t ; for the GRU, it effectively masks the native continuous update gate z_t ; and for the SNN, it regulates the integration of the membrane potential. This unified formulation illustrates that selective updates serve as a backbone-agnostic control layer, effectively decoupling the timing of updates from the specific dynamical laws of the underlying neuron.

B. Efficient Implementation of suGRU

BPTT is often viewed as too slow to scale across long sequences and deep networks. Building on the selective-update concept, we implement *suGRU* so that it executes in a *single* cuDNN GRU pass while realizing a temporal-residual update/carry at each step. We supply an external binary gate $g_t \in \{0, 1\}^H$ ($1 = \text{update}$, $0 = \text{carry}$) and concatenate the *skip drive* ($1 - g_t$) as H additional input channels. Inside the fused GRU we *hard-wire only the z -head* on these extra channels to a fixed diagonal $+C I_H$ (the r/n heads are wired to zero; all other weights remain trainable. More details are explained

in Appendix B.1). This equation represents a z -preactivation shift:

$$\mathbf{z}_t^{\text{pred}} = \mathbf{z}_t^{\text{org}} + C(\mathbf{1} - \mathbf{g}_t),$$

Here, $\mathbf{z}_t^{\text{org}}$ denotes the z -preactivation in the original GRU implementation. so that $g_t = 0$ yields a step *identical* to a standard GRU (exact update), while $g_t = 1$ saturates the z -gate toward 1 and behaves as a carry in the residual form $h_t \approx h_{t-1}$. Gates are produced once per sequence by lightweight, length-agnostic generators (e.g., B-splines with compact support, time-warped sines, or spectral masks) trained with a straight-through estimator. Because no custom control flow is introduced, the entire sequence is executed in a single cuDNN kernel with GRU throughput. The only runtime overhead comes from the $+H$ gate channels. The asymptotic complexity remains $O(T(HD + H^2))$ without adding any extra parameters to the GRU component. As a result, Fig. A2 shows a significant speedup compared to vanilla step-wise updates. The code is available at <https://anonymous.4open.science/r/suGRU-EB5C>.

The same implementation supports *group gating* (one gate shared by a block of units), an *always-on subset* (guaranteeing a live gradient path), and *state expansion* via grouped projections, without breaking cuDNN fusion. In effect, suGRU preserves GRU-level efficiency while converting optimization depth from sequence length to the *number of updates*, enabling scalable BPTT on long sequences at reasonable speed.

B.1. Validating the cuDNN-fused suGRU via the `dense_z` map

Setup (augment the input with a skip-drive). We form an augmented input

$$\hat{\mathbf{x}}_t = \begin{bmatrix} \mathbf{x}_t \\ \mathbf{I}_H - \mathbf{g}_t \end{bmatrix} \in \mathbb{R}^{D+H},$$

where $g_t \in \{0, 1\}^H$ ($1 = \text{update}$, $0 = \text{carry}$). The GRU preactivations for the three heads (reset r , update z , candidate n) are

$$\begin{bmatrix} \mathbf{r}_t^{\text{pre}} \\ \mathbf{z}_t^{\text{pre}} \\ \mathbf{n}_t^{\text{pre}} \end{bmatrix} = \mathbf{W}_{ih} \hat{\mathbf{x}}_t + \mathbf{W}_{hh} \mathbf{h}_{t-1} + \mathbf{b}_{ih} + \mathbf{b}_{hh}, \quad \mathbf{W}_{ih} \in \mathbb{R}^{3H \times (D+H)}, \quad \mathbf{W}_{hh} \in \mathbb{R}^{3H \times H}.$$

Partition \mathbf{W}_{ih} by rows (heads) and columns (real inputs vs. gate channels):

$$\mathbf{W}_{ih} = \begin{bmatrix} \mathbf{W}_x^{(r)} & \mathbf{W}_g^{(r)} \\ \mathbf{W}_x^{(z)} & \mathbf{W}_g^{(z)} \\ \mathbf{W}_x^{(n)} & \mathbf{W}_g^{(n)} \end{bmatrix}, \quad \mathbf{W}_x^{(\cdot)} \in \mathbb{R}^{H \times D}, \quad \mathbf{W}_g^{(\cdot)} \in \mathbb{R}^{H \times H}.$$

Forced wiring on the gate channels. We enforce

$$\mathbf{W}_g^{(r)} = 0, \quad \mathbf{W}_g^{(n)} = 0, \quad \boxed{\mathbf{W}_g^{(z)} = C \mathbf{I}_H}, \quad C < 0,$$

while all other blocks remain trainable. Forced wiring is applied following each training update.

What `dense_z` computes under the wiring. With the above structure, the z -preactivation satisfies

$$\begin{aligned} \mathbf{z}_t^{\text{pre}} &= \mathbf{W}_x^{(z)} \mathbf{x}_t + \mathbf{W}_g^{(z)} (\mathbf{I}_H - \mathbf{g}_t) + \mathbf{W}_h^{(z)} \mathbf{h}_{t-1} + \mathbf{b}^{(z)} \\ &= \underbrace{(\mathbf{W}_x^{(z)} \mathbf{x}_t + \mathbf{W}_h^{(z)} \mathbf{h}_{t-1} + \mathbf{b}^{(z)})}_{=: \mathbf{z}_t^{\text{org}}} + \underbrace{C \mathbf{I}_H}_{\mathbf{W}_g^{(z)}} (\mathbf{I}_H - \mathbf{g}_t) \\ &= \boxed{\mathbf{z}_t^{\text{org}} + C(\mathbf{I}_H - \mathbf{g}_t)}, \end{aligned}$$

where $\mathbf{z}_t^{\text{org}}$ represents the preactivation of the original GRU implementation. Thus, the update gate is effectively modified as

$$\mathbf{z}'_t = \sigma(\mathbf{z}_t^{\text{org}} + C(\mathbf{I}_H - \mathbf{g}_t)),$$

While the r and n heads remain unchanged (with their gate-channel blocks set to zero), the proposal \tilde{h}_t is computed in the same manner as a standard GRU.

suGRU update and comparison with a hard temporal residual. The GRU state update in residual form is

$$\mathbf{h}_t = \mathbf{h}_{t-1} + \mathbf{z}'_t \odot (\tilde{\mathbf{h}}_t - \mathbf{h}_{t-1}).$$

Using $\mathbf{z}'_t = \sigma(\mathbf{z}_t^{\text{org}} + C(\mathbf{I}_H - \mathbf{g}_t))$, the gate signal is obtained:

$$\mathbf{z}'_t = \mathbf{g}_t \sigma(\mathbf{z}_t^{\text{org}}) + (1 - \mathbf{g}_t) \sigma(\mathbf{z}_t^{\text{org}} + C), \text{ where } C < 0.$$

Hence:

- **Update steps** ($g_t = 1$): $\mathbf{z}'_t = \sigma(\mathbf{z}_t^{\text{org}})$ — the step is *identical* to a vanilla GRU update where .
- **Carry steps** ($g_t = 0$): $\mathbf{z}'_t = \sigma(\mathbf{z}_t^{\text{org}} + C\mathbf{I}_H) \rightarrow 0$ — a nonnegative, exponentially small deviation from a perfect carry.

Retention over long carry runs and choice of C . Let $a_t := -z_t^{\text{org}}$ denote the carry margin, so that $1 - z'_t = \sigma(a_t - C)$. Over L consecutive carry steps, the retained mass satisfies

$$\prod_{k=1}^L (1 - z'_{t-k+1}) = \prod_{k=1}^L \sigma(a_{t-k+1} - C) \geq \sigma(a_{\min} - C)^L,$$

whenever $a_t \geq a_{\min}$ holds on carry steps. To ensure that the retained mass after L carries is at least $1 - \rho$, it suffices to choose C such that

$$\sigma(a_{\min} - C)^L \geq 1 - \rho \iff C \leq a_{\min} - \text{logit}((1 - \rho)^{1/L}), \quad \text{logit}(p) := \log \frac{p}{1 - p}.$$

This design aims to bring z'_t closer to 0 in carry steps, thereby facilitating the efficient transmission of h_{t-1} over long carry sequences. The significance of normalization is underscored in this context: by stabilizing the distribution of z_t^{org} , it ensures a steady margin $a_t = -z_t^{\text{org}}$, thus enabling the realization of a consistent retention guarantee with a constant C .

C. Clarifying the constant C_i in Proposition 1

Let $e_i \in \mathbb{R}^H$ denote the i th standard basis vector and define the row-sensitivity of timestep i as

$$r_{t,i} := e_i^\top \frac{\partial h_t}{\partial h_s} \in \mathbb{R}^{1 \times H}.$$

Using the selective update Jacobian $J_t = I + D_t(J_f^t - I)$, the row-sensitivity evolves as

$$r_{t,i} = r_{t-1,i} J_t = \begin{cases} r_{t-1,i}, & g_{t,i} = 0, \\ r_{t-1,i} J_f^t, & g_{t,i} = 1. \end{cases}$$

Thus, when $g_{t,i} = 0$ the row-sensitivity is propagated exactly (no change and no mixing), while cross-coordinate coupling can only enter at update times through multiplication by J_f^t , whose off-diagonal structure mixes coordinates.

Let $\|\cdot\|$ be any induced matrix norm with compatible vector norm. Then

$$\|r_{t,i}\| \leq \|r_{s,i}\| \prod_{\tau \in \mathcal{U}_i(s,t)} \|J_f^\tau\|, \quad r_{s,i} = e_i^\top,$$

which motivates the constant $C_i := \|e_i^\top\|$. Under standard induced norms (e.g., ℓ_2 , ℓ_1 , or ℓ_∞), we have $C_i = 1$. With this definition, all dependence on temporal horizon is captured by the product over update times, and cross-coordinate coupling affects the bound only through the factors $\|J_f^\tau\|$ that appear when $g_{\tau,i} = 1$.

D. Stepwise Result

We first study selective updates in the standard stepwise RNN implementation on well-known synthetic and sequential benchmarks, to isolate the source of the performance gains and to better understand the underlying mechanism.

D.0.1. COPYING-MEMORY TASK

We revisit the well-known Copying-Memory task (Le et al., 2015), where the model observes a short prefix, then T blanks and a delimiter, and must reproduce the prefix after the delimiter, stressing long-range dependency. For sequences with delay T , we track $\|\partial\ell/\partial h_\tau\|$ as a function of temporal distance for both RNN and GRU, and their selective-update variants. With selective updates, in Fig. 2 a), gradient traces remain bounded and nearly parallel as T increases, consistent with the Jacobian structure $J_t = I + D_t(J_f^t - I)$ and Proposition 1, which predicts effective multiplicative depth governed by updates taken rather than input length. On Copying-Memory with $T = 5000$, the gated models converge faster and reach lower loss, indicating time-sparse credit concentrated on update steps and empirically validating the theoretical mechanism.

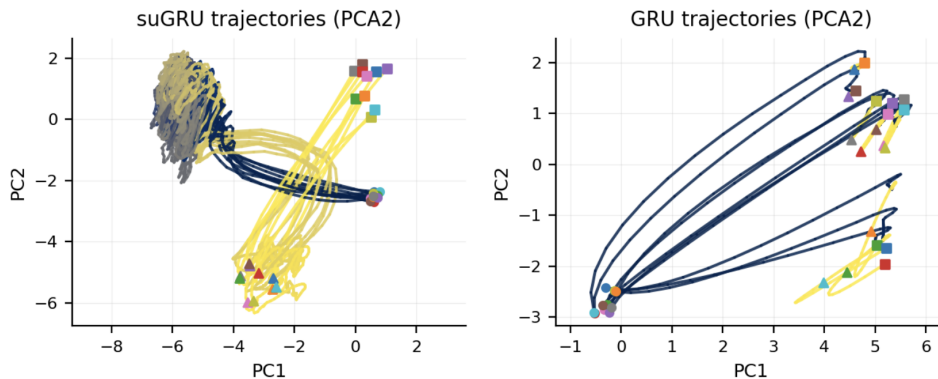


Figure A3. **PCA projection of hidden-state trajectories on Copy-Memory ($T=2000$)**. Starting from the initial hidden state (circle), we follow the recurrent dynamics in the 2D plane; the delimiter timestep is marked by a triangle and the final timestep by a square. Each curve corresponds to one sequence (10 examples in total). Line color encodes normalized time, from early (dark) to late (bright). suGRU (left) exhibits more structured evolution with a clearer separation between delay and recall regimes compared to GRU (right).

Figure A3 projects hidden-state trajectories onto the first two principal components. For long delays ($T = 2000$), GRU states exhibit substantial drift throughout the delay phase, covering a broad region of the PCA plane before recall, whereas suGRU remains tightly clustered during delay and transitions sharply at the delimiter into recall-specific regions, suggesting clearer separation between “maintenance” and “readout” dynamics. Because the copy-task delay is filled with zeros during training, a GRU may exploit this low-entropy segment as an implicit timing cue; replacing the zero delay with random noise at test time confirms this sensitivity: GRU accuracy drops from 27.81% to $\sim 10\%$, while the selective-update model degrades more gradually (85.31% to 48.56%), consistent with selective updates preserving state through the delay and reducing dependence on delay-input statistics.

D.0.2. PSMNIST

Permuted sequential MNIST (psMNIST) is one of the widely used long-range dependency benchmark for recurrent models, where each digit is streamed as a length-784 sequence under a fixed random permutation and the classifier must integrate information across the full horizon. Table 1(a) shows that selective-update recurrence consistently improves classical RNNs and gated variants, with su-RNN and su-GRU reaching the best non-spiking accuracy among the compared baselines and exceeding strong recurrent and

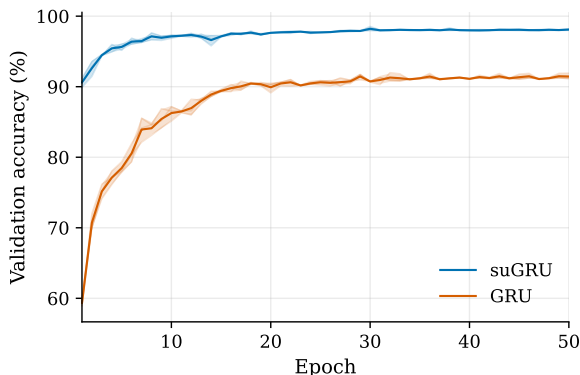


Figure A4. **Learning curves on psMNIST**. Validation accuracy vs. epoch for GRU and suGRU under the same training setting; suGRU converges faster and attains higher accuracy.

Table A1. Validation and test set accuracy for psMNIST.

Model	Validation	Test
FF-baseline	92.37	92.65
RNN-orth	88.70	89.26
RNN-id	85.98	86.13
LSTM	90.01	89.86
LSTM-chrono	88.10	88.43
GRU	92.16	92.39
JANET	92.50	91.94
SRU	92.79	92.49
GORU	86.90	87.00
NRU	95.46	95.38
Phased LSTM	88.76	89.61
LMU	96.97	97.15
su-RNN	97.80	97.76
su-GRU	97.93	98.21
su-LSTM	97.80	97.64
su-GRU(fixed random Rhy)	97.44	97.73
su-GRU(every 3 steps)	10	10.
su-GRU(fixed random)	10.	10.
su-GRU($x > 0$)	nan	nan
su-GRU(learnable $N * T$)	13.86	13.25

(a) Non-spiking neural networks. Ablation study on the basic gate design. *Fixed random Rhythm* uses fixed, randomly initialized parameters for gate generation. *Fixed random* samples gates from a uniform distribution and then binarizes them via a threshold; $x > 0$ gate defines the gate directly from the raw input: whenever a pixel value is positive, the gate is open and the network state is updated.

Model	Validation	Test
GLIF	–	90.47
SRNN	–	94.3
brf-SNN	–	95.2
ASRC-SNN	–	96.62
Rhythm-SNNs	–	96.73
su-SNN	97.21	97.33 ± 0.32

(b) Spiking neural networks

state-space models such as LMU. The ablations isolate the source of the gain: a fixed random rhythmic schedule remains competitive but degrades relative to learned rhythms, while naive gates either collapse to chance or fail to optimize, indicating that correct update timing is essential for stable training. Table 1(b) further shows that the same principle transfers to spiking settings, where su-SNN improves over previous spiking sota performance, suggesting that selective updates provide a general mechanism for long-horizon credit assignment beyond a particular neuron model.

Figure A5 illustrates the separation between *when* the model is permitted to update (gate activity) and *how much* it updates (state increments) along the input stream. The gate maps exhibit a stable, layer-specific temporal structure with a moderate average opening rate, largely consistent across digits, indicating that the model learns a non-uniform compute schedule. In contrast, dh_t concentrates around stroke onsets, offsets, and high-contrast transitions, while extended background regions induce weak increments, consistent with near-carry behavior. Layer 2 shows broader, more distributed update patterns than Layer 1, suggesting that deeper recurrence aggregates local evidence into more global state changes under the same selective-update mechanism.

D.0.3. TIME EFFICIENCY

From the dynamics of selective updates, it could reduce inference cost because inactive coordinates are carried forward without evaluating the recurrent transformation. This conditional execution is not exposed by default in standard PyTorch kernels, which still compute dense GRU updates and apply the mask afterward, so the theoretical savings do not directly translate into wall-clock speed.

To measure the achievable gain under mask-aware execution, we train suRNNs on sequential MNIST and benchmark a stepwise suGRU implemented in C with block-structured gating. Table A2 reports a latency breakdown at 83% sparsity. The dominant savings come from skipping gate and candidate computations, reducing update-gate and candidate-state time to about 8–9% of a dense GRU, and the reset gate to 40%. Overall, the end-to-end step latency drops from 466 ms to 88

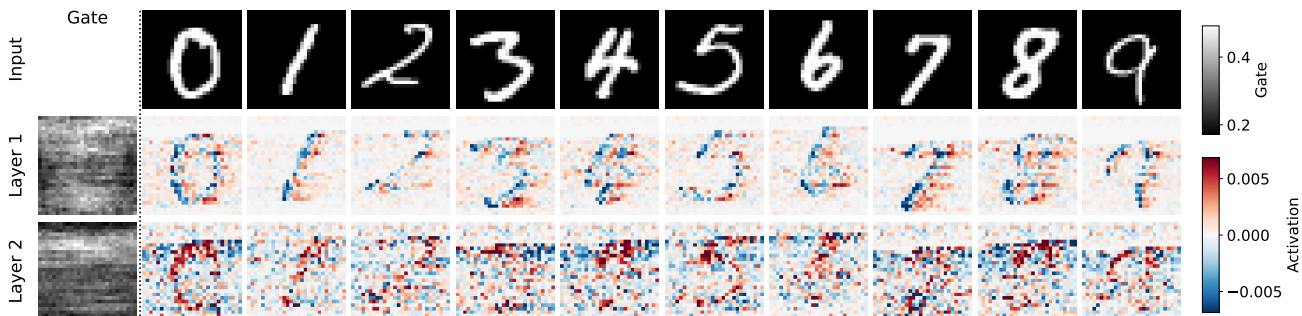


Figure A5. **Selective-update dynamics on sMNIST.** We visualize a two-layer suGRU with 256 hidden units per layer on the sequential MNIST pixel stream. For readability, the 784-step input and the corresponding per-timestep quantities are reshaped to 28×28 . The left column shows the learned gate activity for each layer (gate value averaged over units), while the remaining columns show, for each digit, the input (top) and the signed hidden-state increment $\Delta h_t = h_t - h_{t-1}$ in Layer 1 and Layer 2 (bottom), highlighting when the model actually modifies its recurrent state.

Table A2. Latency comparison between GRU and suGRU with 87% sparsity

Component	GRU (μs)	suGRU (μs)	Ratio
Reset gate r_t	153,411	61,293	0.40
Update gate z_t	154,486	12,659	0.082
Hidden states \tilde{h}_t	154,070	13,429	0.087
Hidden states h_t	4,264	1,018	0.24
Total	466,231	88,399	0.19

ms, a $5.3\times$ speedup. Because computation is explicitly event-triggered by the gate, the selective-update architecture is also naturally aligned with neuromorphic and event-driven hardware, where conditional execution and sparse state updates are first-class constructs.

E. One-pass suGRU

While stepwise selective updates clarify the temporal-residual mechanism, their inherently sequential execution limits throughput, making it difficult to scale to larger models and longer sequences; we therefore turn to a one-pass suGRU formulation that preserves the same gating principle while enabling more efficient training and evaluation.

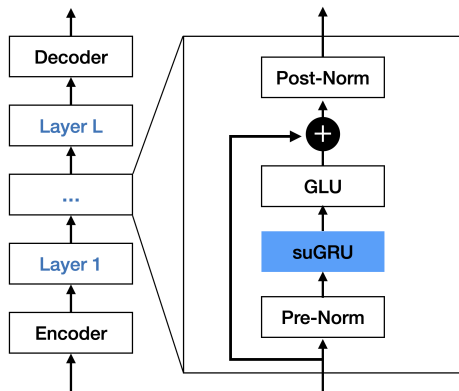


Figure A6. we use this more complex arch to amplify the suGRU power

E.1. Long range Mackey-Glass Prediction

The Mackey–Glass (MG) dataset is a standard chaotic time-series benchmark used to assess a model’s ability to capture nonlinear dynamical structure. We stream one-dimensional observations generated by the MG delay differential equation and train the model to forecast values at varying lead times, predicting between 10 and 1000 steps ahead over sequences of length 5000. The task becomes progressively harder as the prediction horizon increases because chaotic dynamics exhibits Lyapunov instability (as in Fig A7), so small errors in the inferred latent state amplify rapidly, and the model must effectively internalize and roll forward the underlying attractor dynamics.

In this task, we applied the 4 layers RNN with 48 neurons per layer for all four types of RNNs that include LSTM, GUR, SSM and our suGRU. Across all RNN baselines, loss increases steeply with prediction steps: LSTM/GRU perform well at short ranges but deteriorate rapidly beyond ~ 100 steps. The SSM baseline degrades more gradually and remains stronger in the long-range regime, yet still shows clear horizon sensitivity. In contrast, **suGRU** is nearly horizon-invariant from 10 to 1000 steps, maintaining the lowest loss across all horizons. In addition, we could improve the suGRU performance on the short prediction length by forcing some neuron to keep updating every step.

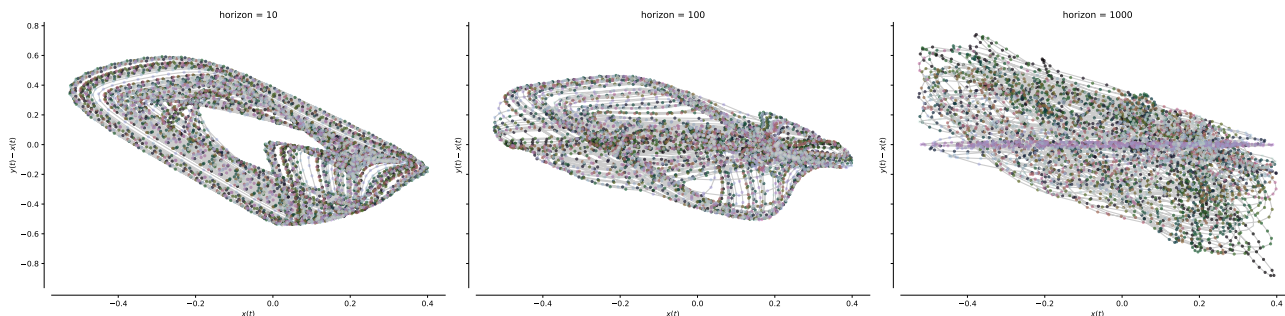


Figure A7. Mackey–Glass rollout geometry across prediction horizons. Phase-space plots of predicted trajectories (delay embedding) overlaid with the true attractor for horizons 10, 100, and 1000, illustrating how long-horizon forecasts progressively deviate from the attractor under chaotic divergence.

E.2. Sequential-cifar10

Sequential CIFAR-10 (sCIFAR) flattens image classification as a long-range sequence problem by streaming the pixels of each image to a recurrent model in scanline order and emitting the label only after the full sequence has been processed. Because most steps are locally redundant, yet early evidence must be preserved until the end, the task is a stringent test of temporal credit assignment and long-term retention. As shown in Table 5, suGRU substantially outperforms both an attention baseline and a range of recurrent alternatives, including unitary and stability-oriented variants. The margin is consistent with the selective-update mechanism, which allows the model to carry state through uninformative spans and concentrate nonlinear computation on informative transitions, improving optimization and long-horizon integration.

Visualization For better interpretability, we reshape the input time sequence (streamed 32×32 scanline order) back into image layout for visualization. Fig A9 shows that the learned gates activate only on a subset of positions, producing piecewise-stable hidden states with sharp transitions at update events, and progressively more structured layer outputs across depth.

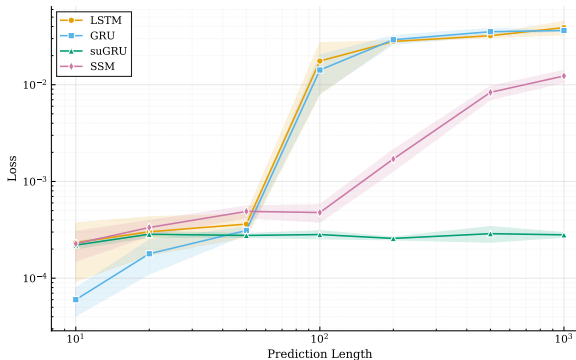


Figure A8. Mackey–Glass multi-step forecasting as a function of prediction steps. The plot reports test loss (log scale) versus ahead time, averaged over seeds; shaded bands indicate variability across 5 runs. suGRU remains stable across horizons up to 10^3 steps, whereas LSTM and GRU exhibit a sharp error increase beyond moderate horizons, and the SSM baseline degrades more gradually but still accumulates error at long lead times.

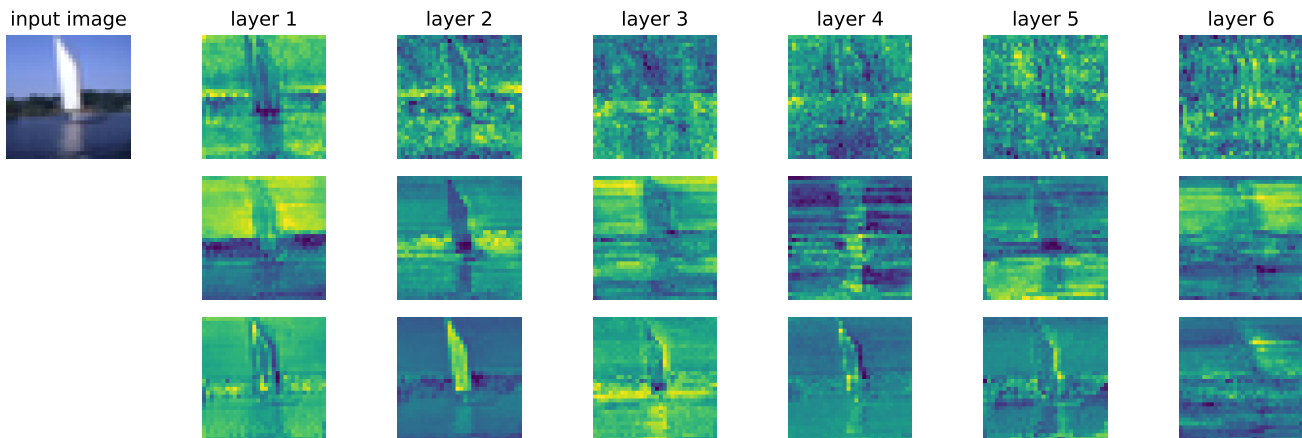


Figure A9. **Selective-update dynamics across depth on sequential CIFAR-10.** The input image is reshaped into a 32×32 scanline sequence and streamed to the model. Columns correspond to stacked recurrent layers (1–6). The top row visualizes the learned binary update gates g_t (averaged over units), the middle row shows the resulting hidden states h_t , and the bottom row shows each layer’s output activations, illustrating how selective updates allocate computation over time and shape representations across depth.

E.3. Experiments Details

Training Setup on WikiText-103. We train our suGRU and self-attention language model on the WikiText-103 dataset. The model architecture consists of a stack of $L = 16$ layers with an embedding dimension of $d_{model} = 300$ and a feed-forward hidden dimension of $d_{ff} = 2100$. We utilize a context window size of 256 tokens. The model is trained using the Adamax optimizer with a batch size of 32 per GPU. We employ a learning rate schedule consisting of a linear warmup for the first 1,000 steps, followed by a cosine decay schedule that anneals the learning rate from a maximum of 5×10^{-4} to zero over the course of 200 epochs. To stabilize training and prevent overfitting, we apply dropout with a probability of 0.1 and initialize weights using a normal distribution with a standard deviation of 0.02. All models are trained in a distributed fashion using PyTorch Distributed Data Parallel (DDP) across multiple GPUs (e.g., $4 \times$ NVIDIA V100/A100), ensuring efficient scaling and synchronization of gradients.